Bioconjugate Chemistry

Article

pubs.acs.org/bc

Synthetically Modified Viral Capsids as Versatile Carriers for Use in Antibody-Based Cell Targeting

Adel M. ElSohly,[†,⊥] Chawita Netirojjanakul,[†,⊥] Ioana L. Aanei,[†,‡] Astraea Jager,[§] Sean C. Bendall,[∥] Michelle E. Farkas,[†] Garry P. Nolan,[§] and Matthew B. Francis*[,†,‡]

[†]Department of Chemistry, University of California, Berkeley, California 94720-1460, United States,

[‡]Materials Sciences Division, Lawrence Berkeley National Laboratories, Berkeley, California 94720-1460, United States,

[§]Baxter Laboratory and Stem Cell Biology, Department of Microbiology and Immunology, Stanford University, Stanford, California 94305, United States

[∥]Stanford Blood Center, Stanford School of Medicine, Palo Alto, California 94304, United States

Supporting Information

ABSTRACT: The present study describes an efficient and reliable method for the preparation of MS2 viral capsids that are synthetically modified with antibodies using a rapid oxidative coupling strategy. The overall protocol delivers conjugates in high yields and recoveries, requires a minimal excess of antibody to achieve modification of more than 95% of capsids, and can be completed in a short period of time. Antibody−capsid conjugates targeting extracellular receptors on human breast cancer cell lines were prepared and characterized. Notably, conjugation to the capsid did not significantly perturb the binding of the antibodies, as indicated by binding affinities similar to those obtained for the parent antibodies. An array of conjugates was synthesized with various reporters on the interior surface of the capsids to be used in cell studies, including fluorescence-based flow cytometry, confocal microscopy, and mass cytometry. The results of these studies lay the foundation for further exploration of these constructs in the context of clinically relevant applications, including drug delivery and in vivo diagnostics.

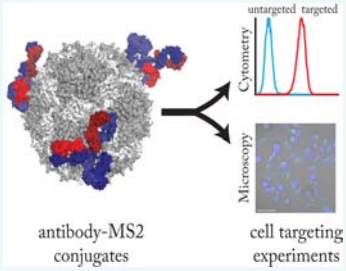

INTRODUCTION

Nanoscale carriers, such as polymers,[1,2] dendrimers,[3,4] inorganic nanoparticles,[5,6] and liposomes,[7,8] have been useful in many applications, including fundamental research, drug delivery, and diagnostic imaging. In addition to these synthetic scaffolds, self-assembled multimeric biomolecular complexes, such as heat shock proteins[9−11] and viral capsids,[12−17] have also shown great promise for the development of next generation imaging and drug delivery agents. The interior cavities and multiple attachment sites of these protein cage scaffolds allow them to house a large amount of imaging or therapeutic payloads, leading to enhancement of the signal intensity and the ability to deliver multiple copies of drug molecules. However, in order to achieve specific detection or delivery, these vehicles must be modified with targeting agents. Correspondingly, studies have increasingly demonstrated the importance of active targeting in achieving appropriate intratumoral localization.[18] Various chemical bioconjugation techniques have played crucial roles in the development of these targeted protein cage nanoparticles using different types of targeting groups, including small molecules,[19,20] nucleic acid aptamers,[15] peptides,[10,21,22] glycans,[23] or antibodies.[10,24] Among the different types of targeting agents, antibodies have been most widely used for a variety of applications due to their general availability as well as high specificity and affinity to targets. Numerous antibodies have been used as research tools or developed into diagnostic or imaging agents; furthermore, a growing number of antibodies (more than 20 to date) are being approved as therapeutic agents targeting specific ligands or receptors.[25−27]

Despite their excellent targeting ability, antibodies have a limited capacity for cargo delivery. Only a small number of modifications can be made on the surface of the antibody without either losing binding to the desired target or reducing efficacy through increased clearance.[28] In addition, drug molecules can induce precipitation of the antibody at high levels of modification due to their hydrophobicity. Great efforts have been dedicated to the optimization of antibody−drug conjugates (ADC), with several now in clinical trials or even available as treatments.[29] The use of viral capsids as delivery vehicles offers a number of advantages to traditional ADC systems. These protein assembles can carry over 100 copies of a given drug molecule, offering significant increases in therapeutic index and allowing the use of less cytotoxic agents. Furthermore, many drugs that are unsuitable for high levels of conjugation to antibodies due to hydrophobicity could be appended inside the capsid without precipitation of the conjugate. Finally, conjugation of drug molecules would not impede epitope binding by virtue of the drug cargo being located inside the capsid.

Received: April 22, 2015
Revised: June 12, 2015
Published: June 15, 2015

DOI: 10.1021/acs.bioconjchem.5b00226
Bioconjugate Chem. 2015, 26, 1590−1596

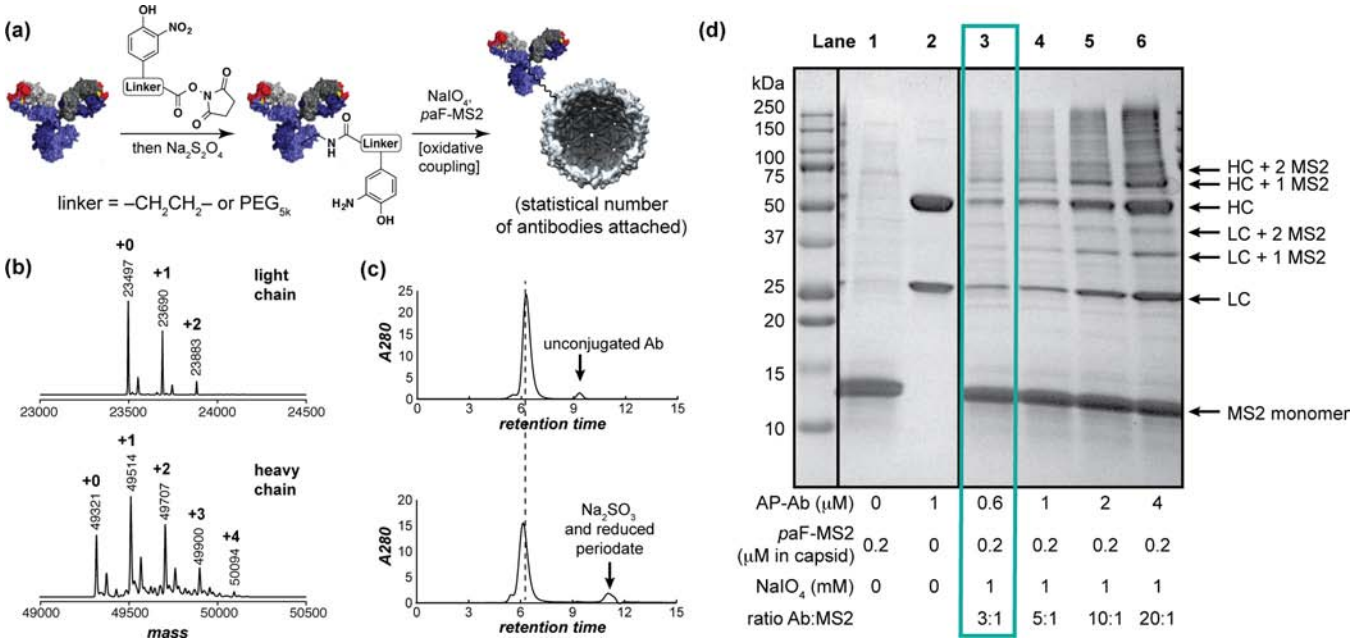

Figure 1. Generation of MS2–antibody conjugates. (a) General synthetic scheme of MS2–antibody conjugates. First, nitrophenol (NP) groups were attached to antibodies via lysine modification using a NP-NHS ester. The nitrophenol groups were then reduced to yield aminophenol-Ab conjugates (AP-Ab) by addition of $Na_2S_2O_4$. The resulting AP-Ab was coupled to *p*aF MS2 via oxidative coupling using $NaIO_4$. (b) LC-MS analysis of humanized anti-HER2 antibodies after lysine modification with 5 equiv of NP-NHS. The light chains (LC) were either unmodified (59%) or modified with one (34%) or two (6%) NP groups. The heavy chains (HC) were modified with 0 (16%), 1 (40%), 2 (31%), 3 (12%), or 4 (1%) NP groups. (c) SEC-HPLC of the oxidative coupling of humanized AP-anti-EGFR and *p*aF-MS2 when a 3:1 ratio of antibody:capsid was used indicates complete consumption of the antibody. The top trace was taken before the addition of sodium periodate, and the bottom trace was taken after addition of sodium sulfite to quench the reaction after 6 min. The peak at ~11.5 min in the latter trace is due to sodium sulfite. (d) SDS-PAGE analysis of MS2-anti-EGFR conjugates using 3, 5, 10, and 20 equiv of Ab with respect to the MS2 capsid concentration. The gel showed conjugation of one or two MS2 monomers to the light and heavy chains of antibodies. More equivalents of Ab resulted in a higher intensity of the modified bands.

Two previous reports have delineated methods for preparing antibody–viral capsid and antibody-heat shock protein conjugates. Both relied on the use of a heterobifunctional maleimide/*N*-hydroxy succinimide (NHS) ester linker,[10,24] and these constructs were successful at specifically targeting and killing cells expressing the receptor of interest when loaded with cytotoxic payloads. These reports did not indicate the effect that conjugation has on the binding affinity of the antibody. Additionally, the synthetic strategies required a large amount of antibody (i.e., high concentration) and extended reaction times.

In this work, we describe the preparation and characterization of a panel of MS2-antibody (MS2-Ab) conjugates using a facile and modular approach that is rapid, results in stoichiometric attachment, and exhibits little interchain cross-linking. Furthermore, the activation of the antibody component prior to coupling yields a stable species that can be stored for subsequent use, a feature that is not possible with maleimides or NHS esters. Biophysical and biological assessments of the MS2-Ab conjugates indicate comparable binding affinity relative to the parent antibodies. Finally, we demonstrate the use of MS2-Ab constructs to detect cell surface receptors via flow cytometry, confocal microscopy, and mass-cytometry.[30,31] The potential of signal enhancement provided by the MS2 scaffold and the high binding specificity and affinity of antibodies can be expanded toward many other applications, including imaging and drug delivery. Moreover, we anticipate that the method presented here can be readily adapted for the generation of a wide range of targeted nanoscale carriers.

RESULTS AND DISCUSSION

Antibody Modification and Attachment to MS2 Viral Capsids. Previous work in our laboratory has demonstrated the utility of genome-free bacteriophage MS2 viral capsids as delivery vehicles for imaging agents[17,32] and therapeutic drugs.[16,33] The capacity of MS2 to load up to 180 copies of small molecules inside the 27 nm icosahedral capsid make it particularly useful for enhancing the intensity of imaging agents or delivering multiple copies of drugs in one carrier. To direct these carriers to specific targets, we have employed several classes of targeting agents, including cyclic peptides,[21] linear peptides,[34] and DNA aptamers.[15] However, monoclonal antibodies (mAbs) provide a large collection of targeting agents that would provide much value to these carriers.

Due to the large sizes of both the antibody (Ab) and MS2 viral capsid, we chose a highly efficient oxidative coupling of aminophenols and anilines to conjugate the two entities. This reaction has been shown to couple two large biomolecules under mild conditions with very short reaction times.[15,21,35,36] Aniline-containing MS2 viral capsids were obtained via unnatural amino acid incorporation of *p*-aminophenylalanine (*p*aF) on the exterior surface.[37,38] The aminophenol moiety was introduced onto the antibodies via non-site-specific lysine modification using a nitrophenol-NHS ester (NP-NHS). When ready for attachment to MS2, the nitro group was reduced chemoselectively to the corresponding aminophenol with sodium dithionite. $NaIO_4$ was then used as the oxidant to couple the two partners (Figure 1a).

DOI: 10.1021/acs.bioconjchem.5b00226
Bioconjugate Chem. 2015, 26, 1590–1596

First, to investigate the possibility of generating MS2-Ab conjugates, a humanized anti-HER2 mAb was used as a model substrate. A screen to find the optimal number of nitrophenol groups to be attached to the mAb revealed that using 5 equiv of NP-NHS was optimal and resulted in ∼40% of the light chains and ∼84% of the heavy chains having at least one NP (Figure 1b and SI Figures 1 and 2) by LC-MS. These levels of modification corresponded to a product distribution wherein 99% of the full-sized mAbs have at least one NP attached (see the Supporting Information for full details). The use of large excesses (>20 equiv) of NP-NHS resulted in extensive interchain cross-linking in the subsequent oxidative coupling step (see SI Figure 3) and did not appreciably improve the coupling conversion. As such, 5 equiv of NP-NHS were used for the generation of AP-mAb in all subsequent experiments. After reducing the nitrophenols to aminophenol groups, these AP-mAb were subjected to trial oxidative coupling reactions with *p*aF-MS2 in 3:1 and 5:1 antibody to capsid ratios, both of which demonstrated clear conjugation to the desired constructs. Importantly, this coupling reaction could be performed on very small scales (10 μL reactions) under high dilution (as low as 200 nM antibody concentration) in less than 10 min (typically under 5 min). Furthermore, this coupling was efficient with humanized (Figure 1) and mouse-derived (SI Figure 3) antibodies, suggesting that differences in the constant regions of antibodies are compatible with this protocol.

To optimize the ratio of mAb per capsid, we varied the number of anti-EGFR mAb equivalents (3, 5, 10, and 20) in the oxidative coupling reaction with *p*aF MS2. The conjugation was confirmed by SDS-PAGE analysis (Figure 1d). Importantly, as more equivalents of antibody were used relative to capsid, an increase in the intensity of bands corresponding to conjugated product was observed, suggesting that increased numbers of antibodies are attached to the capsids. Here, we note that the presence of unmodified light and heavy chain bands is not due to unconjugated antibodies, as any excess was easily removed during purification (vide infra); rather, these bands are due to the chains of the antibody that are not directly attached to the capsid.

To determine the amount of unconjugated Ab remaining after the reactions, we monitored the extent of coupling when 3, 5, 10, and 20 equiv of AP-anti-EGFR are used by high performance liquid chromatography on a size exclusion column (see SEC HPLC traces in SI Figure 4). Reaction mixtures were analyzed prior to the addition of oxidant (precoupling) and following quenching of the periodate with Na_2SO_3 (post-coupling). The reaction of MS2 with 3 equiv of anti-EGFR resulted in no free mAb (Figure 1c), while the reaction with 5 equiv showed only a trace of uncoupled mAb. Increased amounts of free mAb remained when 10 or 20 equiv were added; however, the excess unconjugated mAb could be removed by performing successive spin concentration with molecular weight cutoff (MWCO) of 100 kDa, as confirmed by SEC HPLC. We also found that the MS2-anti-EGFR conjugates derived from a higher number of anti-EGFR equivalents elute at shorter retention times, suggesting an increase in the size of MS2-mAb conjugates relative to the unmodified capsid (SI Figure 5). While these results indicated that the number of equivalents of antibody bound to the capsid can be varied, we favored the 3:1 mAb:MS2 ratio since statistically >95% of the conjugates would be expected to have at least one mAb appended per viral capsid (see Supporting Information and SI Figure 6 for full details). These conditions also require minimal purification as all the antibodies are consumed in the coupling with the MS2 capsid.

Biophysical Characterization of MS2-Ab Conjugates. Given the size change indicated by a shorter SEC HPLC retention time, we pursued a more in-depth size characterization of these constructs. Dynamic light scattering (DLS) measurements of conjugates prepared with an initial 3:1 ratio of mAb:MS2 indicated a size of 30.73 ± 0.80 nm (Figure 2a), only

(a)

Sample	Measured size (nm)
MS2	27.07 ± 1.16
MS2-αEGFR (3 eq)	30.73 ± 0.80
MS2-αEGFR (5 eq)	30.07 ± 0.78
MS2-αEGFR (10 eq)	33.34 ± 1.85
MS2-αEGFR (20 eq)	40.11 ± 0.41

(b)

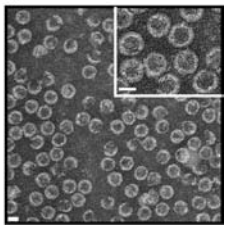

Figure 2. Biophysical characterization of MS2-anti-EGFR conjugates. (a) Size of MS2-anti-EGFR conjugates using varying numbers of equivalents of aminophenol-containing anti-EGFR antibodies as starting materials. Diameters were calculated from an average of three measurements by dynamic light scattering (DLS), shown as size distribution by number, which weights large and small particles equally. (b) Transmission electron micrograph (TEM) images of MS2-Ab conjugates using 3 equiv of AP-anti-EGFR. The capsids were shown to be intact, and their measured diameter was 31 nm. The scale bar represents 20 nm.

∼3 nm larger than the unmodified capsid, which measured 27.07 ± 1.16 nm. This small size difference suggested that the antibodies attached such that the C2 axis of the antibody is tangential, rather than perpendicular, to the surface of the MS2 capsid. Increasing the number of mAb attached to MS2 resulted in an increase in the hydrodynamic radius of the conjugates (Figure 2a). Transmission electron microscopy (TEM) allowed a direct size measurement of 31 nm, consistent with the data obtained from DLS. Importantly, the images showed intact capsid after antibody conjugation and purification (Figure 2b).

Binding Studies of MS2-Ab Conjugates. To test the utility of the MS2-mAb constructs, we analyzed whether the specificity and affinity of the Ab were retained after conjugation to the MS2 capsid. First, Oregon Green 488 dyes (OG) were attached to the mutated Cys (N87C) residue on the interior of MS2 via thiol-maleimide chemistry (SI Figure 7). MS2-OG capsids were then conjugated to a humanized IgG1 mAb that targets epidermal growth factor receptor (EGFR) overexpressed on the cell surface of many cancer types. Using flow cytometry, we analyzed the binding specificity and affinity of the MS2-anti-EGFR conjugates in an EGFR-negative (MCF7 clone 18) and three EGFR-positive (MDA-MB-231, L3.6pl, and HCC1954) human-derived cancer cell lines. The cells were incubated for 45 min on ice with 8 nM MS2 capsid (1.5 μM monomer concentration) in binding buffer (DPBS + 1% FBS). The MS2-anti-EGFR constructs only bound to the EGFR-positive cells, while no binding was observed with the EGFR negative cells (Figure 3a). The untargeted MS2-OG and MS2-OG conjugated to a nonspecific human IgG1 were used as negative controls, neither of which exhibited binding to any of the cell lines tested. This result thus confirmed that the binding of MS2-anti-EGFR conjugates was specifically due to the EGFR/anti-EGFR mAb interaction. Additional experiments using MS2-anti-HER2 on HER2-positive cells are provided in

DOI: 10.1021/acs.bioconjchem.5b00226
Bioconjugate Chem. 2015, 26, 1590−1596

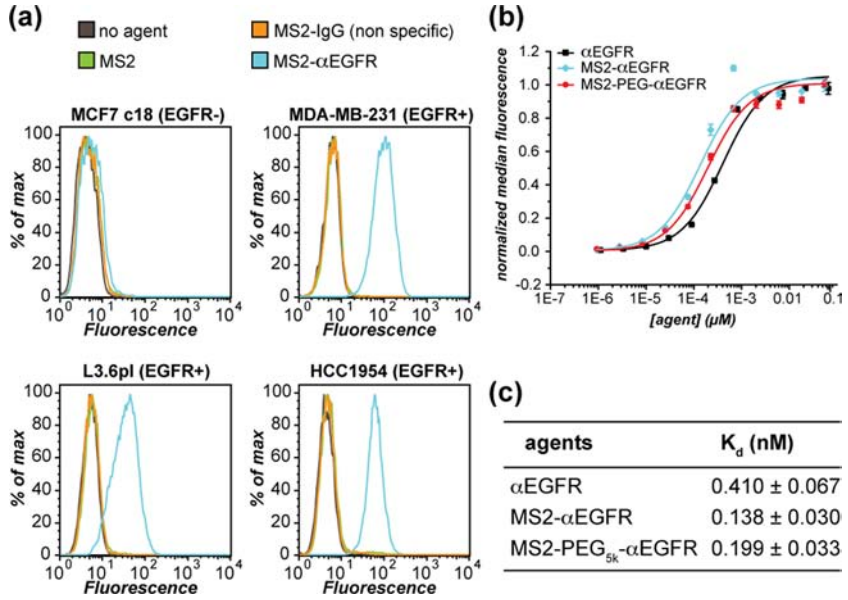

Figure 3. Binding studies of MS2-anti-EGFR antibody conjugates. (a) Flow cytometry analysis of the binding of Oregon Green 488 (OG)-containing MS2-anti-EGFR Ab conjugates to EGFR negative (MCF7 clone 18) and EGFR positive (MDA-MB-231, L3.6pl, and HCC1954) cell lines. The results from flow cytometry showed specific binding of MS2-anti-EGFR conjugates to only the EGFR positive cell lines, while remaining unbound to the EGFR negative cells. MS2-OG and MS2-OG conjugated to nonspecific human IgG1 were used as negative control agents. (b) Comparison of binding affinities of unmodified anti-EGFR antibodies, MS2-anti-EGFR, and MS2-PEG_{5k}-anti-EGFR conjugates. Flow cytometry was used to measure the median fluorescence of MDA-MB-231 cell populations after incubation with the samples. The data were fitted to a single-site binding model. K_d values ± the standard error of each fit are listed in (c).

SI Figure 8. In addition, we prepared MS2-mAb conjugates with a 5 kDa poly(ethylene glycol) (PEG) spacer to investigate whether further improvements to the binding of the MS2-mAb conjugates could be achieved by allowing the antibody to orient more favorably during the binding events. First, nitrophenol-capped 5k-PEG-acid was conjugated to anti-EGFR via lysine modification (see Figure 1a). The nitrophenol groups were reduced to aminophenols (AP), and the AP-PEG-anti-EGFR conjugates were attached to *p*aF MS2 using the same oxidative coupling strategy described above.

Next, we compared the binding affinity of unmodified anti-EGFR antibodies and MS2-anti-EGFR conjugates using MDA-MB-231 breast cancer cells. By fitting the median fluorescence intensity measurement from each point to a single site binding model, we determined the K_d of unmodified anti-EGFR and MS2-anti-EGFR conjugates to be equal to 0.41 ± 0.07 nM and 0.14 ± 0.03 nM, respectively (Figure 3b,c). The K_d of the anti-EGFR mAb was in excellent agreement with another published study of ^{125}I cetuximab binding to EGFR on MDA-MB-231, which reported a K_d of 0.38 nM.[39] Therefore, the conjugation to MS2 was not deleterious to the binding affinity. The binding affinity of MS2-PEG_{5k}-anti-EGFR was assessed by flow cytometry, and the K_d was calculated to be 0.20 ± 0.03 nM, suggesting that the PEG spacer did not decrease the binding affinity substantially relative to MS2-anti-EGFR, and furthermore, targets with sterically demanding epitopes may benefit from such a construct.

Live-Cell Confocal Imaging Studies. Next, we elected to probe the interaction of MS2-mAb conjugates with live cells as a function of time. HCC1954 and MCF7-clone 18 cells were treated with OG-labeled MS2-anti-EGFR and MS2-anti-HER2, respectively, at a concentration of 5.5 nM conjugate for 1 h at 37 °C in DPBS with 1% FBS binding buffer. After incubation, excess conjugates were washed away, and the cells were placed in dye-free media and imaged immediately to provide a 0 h baseline (Figure 4a). The cells were then placed back in an incubator at 37 °C for 1.5 h, and a second round of images were acquired (Figure 4b). After a total of 6 h at 37 °C post-labeling, DAPI was added, and the final images were taken (Figure 4c). Immediately after washing, some signal was already observed in the interior of the cells for both cell lines. As the cells were allowed to interact with surface-bound agent for longer time periods, increased amounts of signal was observed in what appears to be vesicle-like formations, and by 6 h, no discernible signal could be detected on the cell surface. EGFR is known to undergo internalization upon binding to a series of anti-EGFR antibodies, including cetuximab.[40−44] In fact, receptor downregulation and internalization is one of the main mechanisms of action of anti-EGFR therapeutic antibodies.[39] A control experiment utilizing fluorescently labeled anti-EGFR antibodies on HCC1954 cells showed strong labeling of the cell surface (SI Figure 9) at early time points. Intriguingly, the MS2-mAb conjugates were internalized at a higher rate, with most of the signal from agents present within the cells as opposed to on the cell membrane. Taken together, these data suggest that MS2-mAb conjugates targeted to highly overexpressed cell surface receptors may facilitate internalization, possibly through engagement of multiple cell surface receptors by multiple antibodies on the surface of a single capsid. Importantly, control experiments with nontargeted capsids (i.e., either without antibodies or with a nontargeted IgG control on the surface) were not found to bind these cells (SI Figure 10).

Application of MS2-Ab Conjugates in Mass Cytometry. Mass cytometry has emerged as a powerful tool in studying cell signaling events through receptor/protein profiling. This technology uses lanthanide metal isotopes for detection by inductively coupled plasma time-of-flight (ICP-TOF) mass spectrometry, thus allowing as many as 100

DOI: 10.1021/acs.bioconjchem.5b00226
Bioconjugate Chem. 2015, 26, 1590−1596

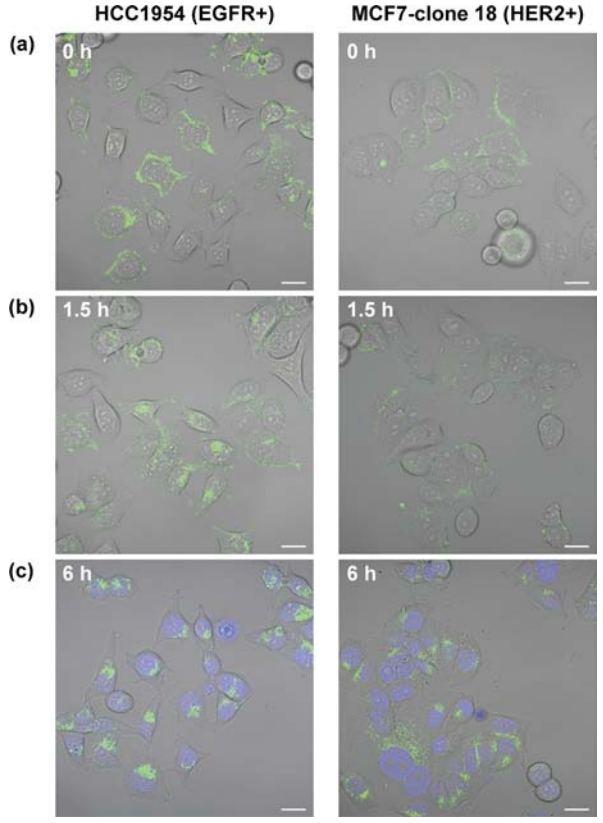

Figure 4. Live-cell confocal microscopy studies of MS2-Ab binding to breast cancer cells. (a) HCC1954 (EGFR+) and MCF7-clone 18 (HER2+) cells were incubated with fluorescently labeled MS2-anti-EGFR and MS2-anti-HER2, respectively, at a concentration of 5.5 nM capsid for 1 h at 37 °C. The cells were washed, placed in fresh dye-free media, and imaged immediately. After imaging, the cells were incubated at 37 °C in the absence of further agent for 1.5 h and were subsequently imaged (b). After a total of 6 h post-incubation at 37 °C, DAPI was added, and the final images were taken (c). Rapid internalization is observed in both cell lines, with the majority of the signal localized inside the cell even 1.5 h after removal of the unbound agent. The scale bars represent 50 μm.

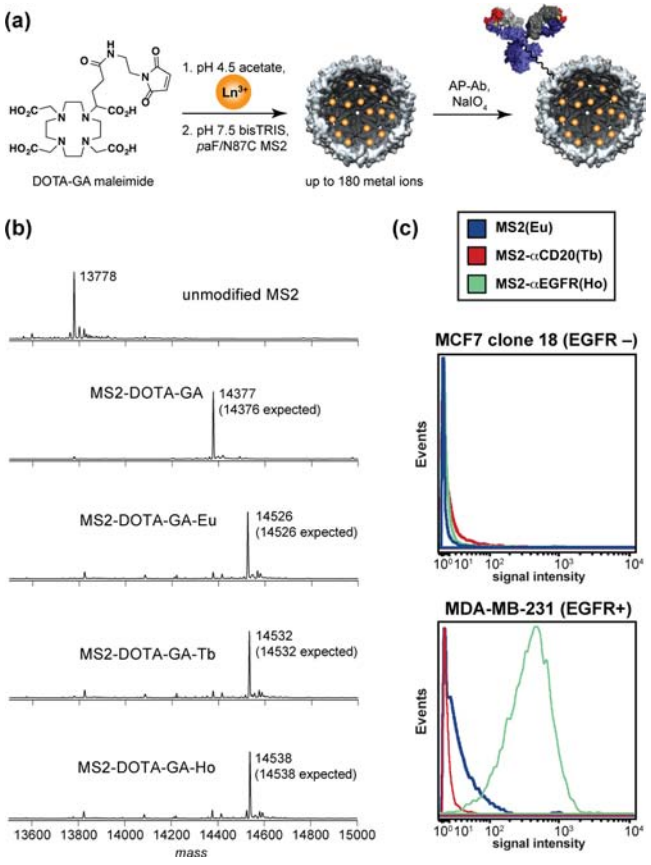

Figure 5. Mass cytometry analysis of binding interactions of lanthanide-chelated agents with cells. (a) Synthetic scheme summarizing synthesis of lanthanide-containing MS2-Ab conjugates. In situ chelation and conjugation of the lanthanide with DOTA-GA maleimide and subsequent oxidative coupling delivers the desired conjugate. (b) LC-MS characterization of the MS2-lanthanide constructs demonstrating that near quantitative conversion occurs. All spectra are reconstructed, and the values represent $[M + H]^+$ ions. (c) Mass cytometry using MCF-7 clone 18 (EGFR and CD20 negative) and MDA-MB-231 (EGFR positive, CD20 negative) costained with a panel of agents. Graphs are plotted as channel overlays of histograms with an arcsinh of 45 applied to all data sets. High levels of staining were only observed for agents displaying EGFR antibodies with EGFR positive cells. Additional controls and cell lines are included in SI Figure 11.

parameters to be measured simultaneously.[45] This number represents a dramatic increase over traditional fluorescence-based flow cytometry, which is limited to ~15 channels due to spectral overlap. In addition, when using lanthanide ions for detection, there is zero background signal from endogenous sources, which provides high sensitivity over a large dynamic range. Here, we took advantage of the MS2 capsid as a vehicle capable of carrying a large number of metal ions for specific detection of proteins of interest in mass cytometry.

As a proof of concept, we generated a series of MS2-lanthanide mass cytometry staining reagents, including MS2-(Ho)-anti-EGFR, MS2(Ho)-PEG_{5k}-anti-EGFR, MS2(Eu) (untargeted control), and MS2(Tb)-anti-CD20 (negative control). These constructs were prepared by initial chelation of the lanthanide ion of interest with DOTA-GA-maleimide followed by in situ conjugation to the interior cysteines of the MS2 capsid (Figure 5a). The use of the DOTA-GA chelator proved optimal (as compared to DOTA-maleimide) in the development of this one-pot procedure due to the increased solubility of the lanthanide-chelated species in aqueous solutions (Figure 5b). Subsequent conjugation of the antibodies provided the desired panel of agents. For these studies, we used HCC1954 and MDA-MB-231 cell lines, which are known to overexpress the EGFR and not the CD20 receptor. The MCF7 clone 18 cell line was used as the negative control. Cells were stained with a mixture of 3 agents that included either MS2(Ho)-anti-EGFR or MS2(Ho)-PEG_{5k}-anti-EGFR as the targeted reporter in addition to MS2(Eu) and MS2(Tb)-anti-CD20 as controls. The simultaneous treatment with multiple agents dramatically reduces the number of samples to be examined and limits the variability among them.

Consistent with our fluorescence-based flow cytometry results, we observed specific binding of the targeted agents to the cells expressing EGFR (Figure 5c). In addition, these reporters provided signal on par with the positive control antibody–polymeric chelators when treated at similar concentrations (see SI Figure 11). Continuing studies are focused on providing substantial signal increases through encapsulation of lanthanide nanoparticles inside targeted MS2 capsids[46] to

DOI: 10.1021/acs.bioconjchem.5b00226
Bioconjugate Chem. 2015, 26, 1590–1596

detect single binding events within individual cells in complex cell populations.

CONCLUSIONS

The work presented describes a rapid and facile strategy for the attachment of full-length antibodies to the exterior surfaces of genome-free MS2 viral capsids. This method of attachment does not require a large excess of the antibody targeting moiety, mitigating some of the costs associated with obtaining targeted agents through other methods. The conjugates maintain the targeting affinity and specificity of the parent antibodies and have physical properties similar to those of the unmodified capsids. The hollow protein shells provide the advantage of various cargo (dyes, chelators, drug molecules) being attached to the interior surface without affecting the overall binding properties of the construct. MS2-mAb have been used to detect targets of interest via different methodologies, such as confocal microscopy, flow cytometry, and mass cytometry. While such constructs may be immunogenic, the labeling approach utilized herein provides the opportunity to utilize PEG molecules or "self-peptides"[47] to help mitigate these effects, and work in these areas is currently underway in our laboratories. Through extensive optimization of the reaction conditions and characterization of the corresponding conjugates, these studies have laid the foundation for the use of MS2-mAb as targeted in vivo imaging agents and drug delivery systems.

ASSOCIATED CONTENT

Supporting Information

Full experimental details and figures. The Supporting Information is available free of charge on the ACS Publications website at DOI: 10.1021/acs.bioconjchem.5b00226.

AUTHOR INFORMATION

Corresponding Author

*E-mail: mbfrancis@berkeley.edu.

Author Contributions

⊥Adel M. ElSohly and Chawita Netirojjanakul contributed equally to this work.

Notes

The authors declare no competing financial interest.

ACKNOWLEDGMENTS

These studies were funded by the DOD Breast Cancer Research Program (Grants BC061995, BC100159, and W81XWH-14-0400 to M.B.F., M.E.F., and A.M.E., respectively) and the W.M. Keck Foundation. C.N. was supported by a Howard Hughes Medical Institute International Student Research Fellowship. I.L.A. was supported by the Genentech Fellowship through the U.C. Berkeley Chemical Biology program. G.P.N. was supported by grants from the NIH (U19 AI057229, U54CA149145, N01−HV-00242, 1U19AI100627, 5R01AI07372405, R01CA184968, 1 R33 CA183654, R33 CA183692), NIH-Baylor Research Institute (41000411217), NIH-Northrop Grumman Corp. (7500108142), CIRM (DR1-01477), DOD (OC110674, 11491122), the European Commission (Health.2010.1.2-1), FDA (HHSF223201210194C), and the Bill and Melinda Gates Foundation (OPP 1017093). LC-MS instrumentation was acquired with National Institutes of Health Grant 1S10RR022393-01. The authors thank Stacy Capehart for acquisition of the TEM images in this study.

REFERENCES

(1) Liu, S., Maheshwari, R., and Kiick, K. L. (2009) Polymer-based therapeutics. *Macromolecules 42*, 3−13.
(2) Srivastava, A., O'Connor, I. B., Pandit, A., and Gerard Wall, J. (2014) Polymer-antibody fragment conjugates for biomedical applications. *Prog. Polym. Sci. 39*, 308−329.
(3) Svenson, S., and Tomalia, D. A. (2005) Dendrimers in biomedical applications–reflections on the field. *Adv. Drug Delivery Rev. 57*, 2106−2129.
(4) Lee, C. C., MacKay, J. A., Fréchet, J. M. J., and Szoka, F. C. (2005) Designing dendrimers for biological applications. *Nat. Biotechnol. 23*, 1517−1526.
(5) Gao, X., Cui, Y., Levenson, R. M., Chung, L. W. K., and Nie, S. (2004) In vivo cancer targeting and imaging with semiconductor quantum dots. *Nat. Biotechnol. 22*, 969−976.
(6) Liong, M., Lu, J., Kovochich, M., Xia, T., Ruehm, S. G., Nel, A. E., Tamanoi, F., and Zink, J. I. (2008) Multifunctional inorganic nanoparticles for imaging, targeting, and drug delivery. *ACS Nano 2*, 889−896.
(7) Torchilin, V. P. (2005) Recent advances with liposomes as pharmaceutical carriers. *Nat. Rev. Drug Discovery 4*, 145−160.
(8) Tiwari, G., Tiwari, R., Sriwastawa, B., Bhati, L., Pandey, S., Pandey, P., and Bannerjee, S. K. (2012) Drug delivery systems: An updated review. *Int. J. Pharm. Investig. 2*, 2−11.
(9) Flenniken, M. L., Liepold, L. O., Crowley, B. E., Willits, D. A., Young, M. J., and Douglas, T. (2005) Selective attachment and release of a chemotherapeutic agent from the interior of a protein cage architecture. *Chem. Commun.*, 447−449.
(10) Flenniken, M. L., Willits, D. A., Harmsen, A. L., Liepold, L. O., Harmsen, A. G., Young, M. J., and Douglas, T. (2006) Melanoma and lymphocyte cell-specific targeting incorporated into a heat shock protein cage architecture. *Chem. Biol. 13*, 161−170.
(11) Suci, P., Kang, S., Gmür, R., Douglas, T., and Young, M. (2010) Targeted delivery of a photosensitizer to aggregatibacter actinomycetemcomitans biofilm. *Antimicrob. Agents Chemother. 54*, 2489−2496.
(12) Wang, Q., Kaltgrad, E., Lin, T., Johnson, J. E., and Finn, M. G. (2002) Natural supramolecular building blocks: wild-type cowpea mosaic virus. *Chem. Biol. 9*, 805−811.
(13) Douglas, T., and Young, M. (2006) Viruses: making friends with old foes. *Science 312*, 873−875.
(14) Kovacs, E. W., Hooker, J. M., Romanini, D. W., Holder, P. G., Berry, K. E., and Francis, M. B. (2007) Dual-surface-modified bacteriophage MS2 as an ideal scaffold for a viral capsid-based drug delivery system. *Bioconjugate Chem. 18*, 1140−1147.
(15) Tong, G. J., Hsiao, S. C., Carrico, Z. M., and Francis, M. B. (2009) Viral capsid DNA aptamer conjugates as multivalent cell-targeting vehicles. *J. Am. Chem. Soc. 131*, 11174−11178.
(16) Wu, W., Hsiao, S. C., Carrico, Z. M., and Francis, M. B. (2009) Genome-free viral capsids as multivalent carriers for taxol delivery. *Angew. Chem., Int. Ed. 48*, 9493−9497.
(17) Garimella, P. D., Datta, A., Romanini, D. W., Raymond, K. N., and Francis, M. B. (2011) Multivalent, high-relaxivity MRI contrast agents using rigid cysteine-reactive gadolinium complexes. *J. Am. Chem. Soc. 133*, 14704−14709.
(18) Bertrand, N., Wu, J., Xu, X., Kamaly, N., and Farokhzad, O. C. (2014) Cancer nanotechnology: the impact of passive and active targeting in the era of modern cancer biology. *Adv. Drug Delivery Rev. 66*, 2−25.
(19) Destito, G., Yeh, R., Rae, C. S., Finn, M. G., and Manchester, M. (2007) Folic acid-mediated targeting of cowpea mosaic virus particles to tumor cells. *Chem. Biol. 14*, 1152−1162.
(20) Ren, Y., Wong, S. M., and Lim, L.-Y. (2007) Folic acid-conjugated protein cages of a plant virus: a novel delivery platform for doxorubicin. *Bioconjugate Chem. 18*, 836−843.
(21) Behrens, C. R., Hooker, J. M., Obermeyer, A. C., Romanini, D. W., Katz, E. M., and Francis, M. B. (2011) Rapid chemoselective bioconjugation through oxidative coupling of anilines and aminophenols. *J. Am. Chem. Soc. 133*, 16398−16401.

DOI: 10.1021/acs.bioconjchem.5b00226
Bioconjugate Chem. 2015, 26, 1590−1596

(22) Hovlid, M. L., Steinmetz, N. F., Laufer, B., Lau, J. L., Kuzelka, J., Wang, Q., Hyypiä, T., Nemerow, G. R., Kessler, H., Manchester, M., et al. (2012) Guiding plant virus particles to integrin-displaying cells. *Nanoscale 4*, 3698−3705.
(23) Rhee, J.-K., Baksh, M., Nycholat, C., Paulson, J. C., Kitagishi, H., and Finn, M. G. (2012) Glycan-targeted virus-like nanoparticles for photodynamic therapy. *Biomacromolecules 13*, 2333−2338.
(24) Brown, W. L., Mastico, R. a., Wu, M., Heal, K. G., Adams, C. J., Murray, J. B., Simpson, J. C., Lord, J. M., Taylor-Robinson, A. W., and Stockley, P. G. (2002) RNA Bacteriophage capsid-mediated drug delivery and epitope presentation. *Intervirology 45*, 371−380.
(25) Weiner, L. M., Surana, R., and Wang, S. (2010) Monoclonal antibodies: versatile platforms for cancer immunotherapy. *Nat. Rev. Immunol. 10*, 317−327.
(26) Jiang, X.-R., Song, A., Bergelson, S., Arroll, T., Parekh, B., May, K., Chung, S., Strouse, R., Mire-Sluis, A., and Schenerman, M. (2011) Advances in the assessment and control of the effector functions of therapeutic antibodies. *Nat. Rev. Drug Discovery 10*, 101−111.
(27) Trail, P. (2013) Antibody drug conjugates as cancer therapeutics. *Antibodies 2*, 113−129.
(28) Hamblett, K. J., Senter, P. D., Chace, D. F., Sun, M. M. C., Lenox, J., Cerveny, C. G., Kissler, K. M., Bernhardt, S. X., Kopcha, A. K., Zabinski, R. F., et al. (2004) Effects of drug loading on the antitumor activity of a monoclonal antibody drug conjugate. *Clin. Cancer Res. 10*, 7063−7070.
(29) Chari, R. V. J., Miller, M. L., and Widdison, W. C. (2014) Antibody−drug conjugates: an emerging concept in cancer therapy. *Angew. Chem., Int. Ed. 53*, 3796−3827.
(30) Lou, X., Zhang, G., Herrera, I., Kinach, R., Ornatsky, O., Baranov, V., Nitz, M., and Winnik, M. A. (2007) Polymer-based elemental tags for sensitive bioassays. *Angew. Chem., Int. Ed. 46*, 6111−6114.
(31) Bandura, D. R., Baranov, V. I., Ornatsky, O. I., Antonov, A., Kinach, R., Lou, X., Pavlov, S., Vorobiev, S., Dick, J. E., and Tanner, S. D. (2009) Mass cytometry: technique for real time single cell multitarget immunoassay based on inductively coupled plasma time-of-flight mass spectrometry. *Anal. Chem. 81*, 6813−6822.
(32) Farkas, M. E., Aanei, I. L., Behrens, C. R., Tong, G. J., Murphy, S. T., O'Neil, J. P., and Francis, M. B. (2013) PET Imaging and biodistribution of chemically modified bacteriophage MS2. *Mol. Pharmaceutics 10*, 69−76.
(33) Stephanopoulos, N., Tong, G. J., Hsiao, S. C., and Francis, M. B. (2010) Dual-surface modified virus capsids for targeted delivery of photodynamic agents to cancer cells. *ACS Nano 4*, 6014−6020.
(34) Obermeyer, A. C., Capehart, S. L., Jarman, J. B., and Francis, M. B. (2014) Multivalent viral capsids with internal cargo for fibrin imaging. *PLoS One 9*, e100678.
(35) Hooker, J. M., Esser-Kahn, A. P., and Francis, M. B. (2006) Modification of aniline containing proteins using an oxidative coupling strategy. *J. Am. Chem. Soc. 128*, 15558−15559.
(36) Netirojjanakul, C., Witus, L. S., Behrens, C. R., Weng, C.-H., Iavarone, A. T., and Francis, M. B. (2013) Synthetically modified Fc domains as building blocks for immunotherapy applications. *Chem. Sci. 4*, 266−272.
(37) Carrico, Z. M., Romanini, D. W., Mehl, R. A., and Francis, M. B. (2008) Oxidative coupling of peptides to a virus capsid containing unnatural amino acids. *Chem. Commun.*, 1205−1207.
(38) Mehl, R. A., Anderson, J. C., Santoro, S. W., Wang, L., Martin, A. B., King, D. S., Horn, D. M., and Schultz, P. G. (2003) Generation of a bacterium with a 21 amino acid genetic code. *J. Am. Chem. Soc. 125*, 935−939.
(39) Patel, D., Lahiji, A., Patel, S., Franklin, M., Jimenez, X., Hicklin, D. J., and Kang, X. (2007) Monoclonal antibody cetuximab binds to and down-regulates constitutively activated epidermal growth factor receptor vIII on the cell surface. *Anticancer Res. 27*, 3355−3366.
(40) Sunada, H., Magun, B. E., Mendelsohn, J., and MacLeod, C. L. (1986) Monoclonal antibody against epidermal growth factor receptor is internalized without stimulating receptor phosphorylation. *Proc. Natl. Acad. Sci. U. S. A. 83*, 3825−3829.
(41) Fan, Z., Lu, Y., Wu, X., and Mendelsohn, J. (1994) Antibody-induced epidermal growth factor receptor dimerization mediates inhibitionof autocrine proliferation oAf 431 squamous carcinoma cells. *J. Biol. Chem. 269*, 27595−27602.
(42) Harding, J., and Burtness, B. (2005) Cetuximab: an epidermal growth factor receptor chemeric human-murine monoclonal antibody. *Drugs of today (Barcelona, Spain : 1998) 41*, 107−127.
(43) Perez-Torres, M., Guix, M., Gonzalez, A., and Arteaga, C. L. (2006) Epidermal growth factor receptor (EGFR) antibody down-regulates mutant receptors and inhibits tumors expressing EGFR mutations. *J. Biol. Chem. 281*, 40183−40192.
(44) Perera, R. M., Zoncu, R., Johns, T. G., Pypaert, M., Lee, F.-T., Mellman, I., Old, L. J., Toomre, D. K., and Scott, A. M. (2007) Internalization, intracellular trafficking, and biodistribution of monoclonal antibody 806: a novel anti-epidermal growth factor receptor antibody1. *Neoplasia 9*, 1099−1110.
(45) Bendall, S. C., Simonds, E. F., Qiu, P., Amir, E. D., Krutzik, P. O., Finck, R., Bruggner, R. V., Melamed, R., Trejo, A., Ornatsky, O. I., et al. (2011) Single-cell mass cytometry of differential immune and drug responses across a human hematopoietic continuum. *Science 332*, 687−696.
(46) Capehart, S. L., Coyle, M. P., Glasgow, J. E., and Francis, M. B. (2013) Controlled integration of gold nanoparticles and organic fluorophores using synthetically modified MS2 viral capsids. *J. Am. Chem. Soc. 135*, 3011−3016.
(47) Rodriguez, P. L., Harada, T., Christian, D. A., Pantano, D. A., Tsai, R. K., and Discher, D. E. (2013) Minimal "self" peptides that inhibit phagocytic clearance and enhance delivery of nanoparticles. *Science 339*, 971−975.

DOI: 10.1021/acs.bioconjchem.5b00226
Bioconjugate Chem. 2015, 26, 1590−1596